Stoch Environ Res Risk Assess (2010) 24:29–46
DOI 10.1007/s00477-008-0297-4

ORIGINAL PAPER

Sea level fluctuations on the east coast of Taiwan that overlie continental shelf break

David Ching-Fang Shih · Yue-Gau Chen · Gwo-Fong Lin · Yih-Min Wu · Yee-Ping Jia · Chih-Ming Ma

Published online: 19 December 2008

Abstract Captured CO_2 could be deliberately injected into the ocean at great depth, where most of it would remain isolated from the atmosphere for centuries. CO_2 can be transported via pipeline or ship for release in the ocean or on the sea floor. No matter what for medium depth or deep sea, it appears that a potential area exists between 122–122.5°E and 21.8–22.3°N for CO_2 sequestration. The east coast of Taiwan can be a candidate for CO_2 temporary storage or transmitted plant. To have whole picture of assessment of sea level fluctuation, a completed statistical summary of seasonal sea level at six tidal gauge stations along the east coast of Taiwan is provided herein. Seasonal sea level time series is analyzed using spectral analysis in frequency domain to identify periodic component and phase propagation, especially for the astronomical-driven tidal effects. It identifies that the semi-diurnal and diurnal components in the resultant time series are related to astronomical tides M_2, and K_1 and O_1, respectively. It demonstrates a full analysis of sea level variations, and results can be useful when construction of testing or operating facilities on sea surface becomes desirable in the future.

Keywords Sea level · Continental shelf · Spectral analysis · East coast of Taiwan · CO_2 sequestration

D. C.-F. Shih · Y.-G. Chen · Y.-M. Wu · Y.-P. Jia
Department of Geosciences,
National Taiwan University,
1 Sec.4, Roosevelt Rd.,
Taipei 10617, Taiwan, ROC

G.-F. Lin
Department of Civil Engineering,
National Taiwan University,
1 Sec.4, Roosevelt Rd.,
Taipei 10617, Taiwan, ROC

D. C.-F. Shih (✉) · C.-M. Ma
Institute of Nuclear Energy Research, AEC,
P.O. Box 3-7, Longtan 32546, Taiwan, ROC
e-mail: cfshih@iner.gov.tw

1 Introduction

In Taiwan, CO_2 release is preliminarily projected to be 0.332–0.531 Gt from 2010 to 2030 with an average amount of 6.473 Gt within this duration. Direct ocean injection of CO_2 is one of several approaches under consideration to sequester carbon dioxide in order to stabilize increasing content of atmospheric CO_2. A potential CO_2 storage option is to inject the captured CO_2 directly into the deep ocean at depths greater than 1,000 m or more, where most of it could be isolated from the atmosphere for centuries. This can be achieved by transporting CO_2 through pipelines or ships to an ocean storage site where it is injected into the water column of the ocean or at the sea floor. The dissolved and dispersed CO_2 would subsequently become a part of the global carbon cycle. Ocean storage has not yet been deployed or demonstrated with a pilot scale so far, and is still in the research stage. However, there have been small scale field experiments and 25 years of theoretical, laboratory and modeling studies for intentional ocean storage of CO_2. At typical pressures and temperatures that exist in the ocean, pure CO_2 would be a gas above approximately 500 m and a liquid below that depth. Between about 500 and 2,700 m of depth, liquid CO_2 is lighter than sea water (IPCC 2005), while deeper than 3,000 m, CO_2 is denser than sea water. The buoyancy of CO_2 released into the ocean determines whether released CO_2 rises or falls in the ocean column. In the gas phase, CO_2 is lighter than sea water and rises. In the liquid phase CO_2 is a highly compressible fluid as compared to sea water. A fully formed crystalline CO_2 hydrate is denser than sea water and will become a sinking mass (Aya et al. 2003); formation of hydrate can thus aid storage of ocean CO_2 storage by rapid transport to depth, and by slowing dissolution. It may also create a nuisance by impeding flow in pipelines or at injectors. Studies on the engineering issues of ocean CO_2 storage have been published for cases where CO_2 is delivered from a power plant located on shore by either ship to an offshore injection platform injection ship, or pipeline running on the sea floor to an injection nozzle. In the future, CO_2 recovered from the power plants can be designed and transported by a CO_2 tanker to a single floating discharge platform for injection at a depth of 3,000 m. In some cases, concept and technology for dilution type at medium depth ($\sim$1,500 m) or lake type at deep depth (>3,000 m) for CO_2 ocean sequestration have been conducted (Brewer et al. 1998, 2000, 2002, 2005; Nakashiki 1997; Ozaki 1997). Marine supporting system on the sea surface or at deep depths needs to be investigated drastically; it will be the most important works in the preliminary assessment stage.

Taiwan lies about 150 km to the east of the Fukien coast of the mainland China, and is separated from the latter by the Taiwan Strait (Fig. 1). Geographically, Taiwan is represented by the main island with thirteen islands and scattered islets. Taiwan is a member of the Ryukyu-Taiwan-Luzon arc chain rimming the western border of the Pacific Ocean (Shih et al. 2008a). The tectonic evolution of Taiwan can be attributed either to the development of classic geosynclinal cycles or to the interaction of crustal plates. Taiwan is formed by a

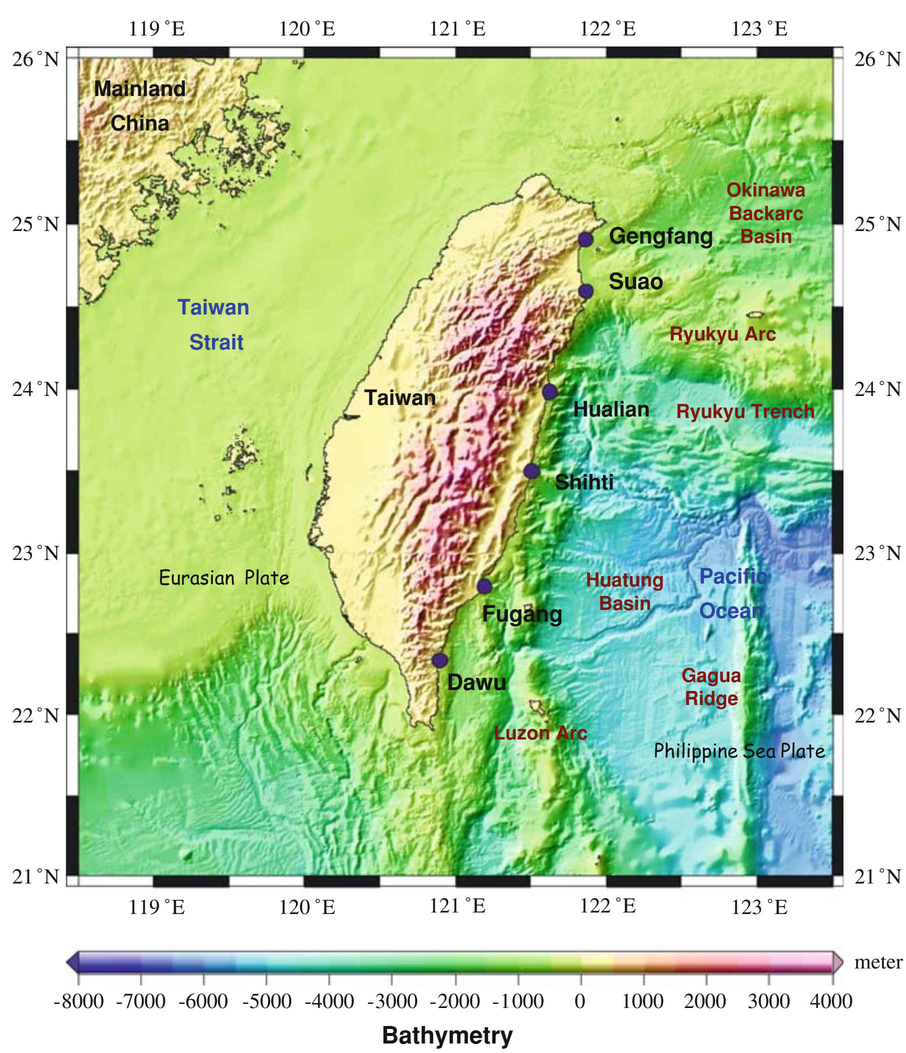

Fig. 1 Map shows tide gauge station along east coast of Taiwan; marine topography are also demonstrated with color scale

Table 1 Tide gauge station

Station title	Latitude, N	Longitude, E	Distance to the next station (km)
Gengfang	24°54′26″	121°51′43″	34.86
Suao	24°35′33″	121°52′02″	72.20
Hualian	23°58′49″	121°37′23″	55.08
Shihti	23°29′41″	121°30′22″	84.32
Fugang	22°47′27″	121°11′32″	58.74
Dawu	22°20′14″	120°53′46″	

Distance from Gengfang to Dawu is 305.20 km

typical mobile or orogenic Cenozoic geosynclinal deposition on a pre-Tertiary metamorphic basement filled with Tertiary sediments to a thickness of more than 10,000 m. Main island of Taiwan is situated on the junction between the continental Eurasian Plate on the west and the oceanic Philippine Sea Plate on the east (Fig. 1). The east coast of Taiwan apparently located on the break of continental shelf of Eurasian Plate. It shows that there are potential areas with depths greater than 3,000 m between 122–122.5°E and 21.8–22.3°N on account of its isolated and flat topography. This range seems to be a

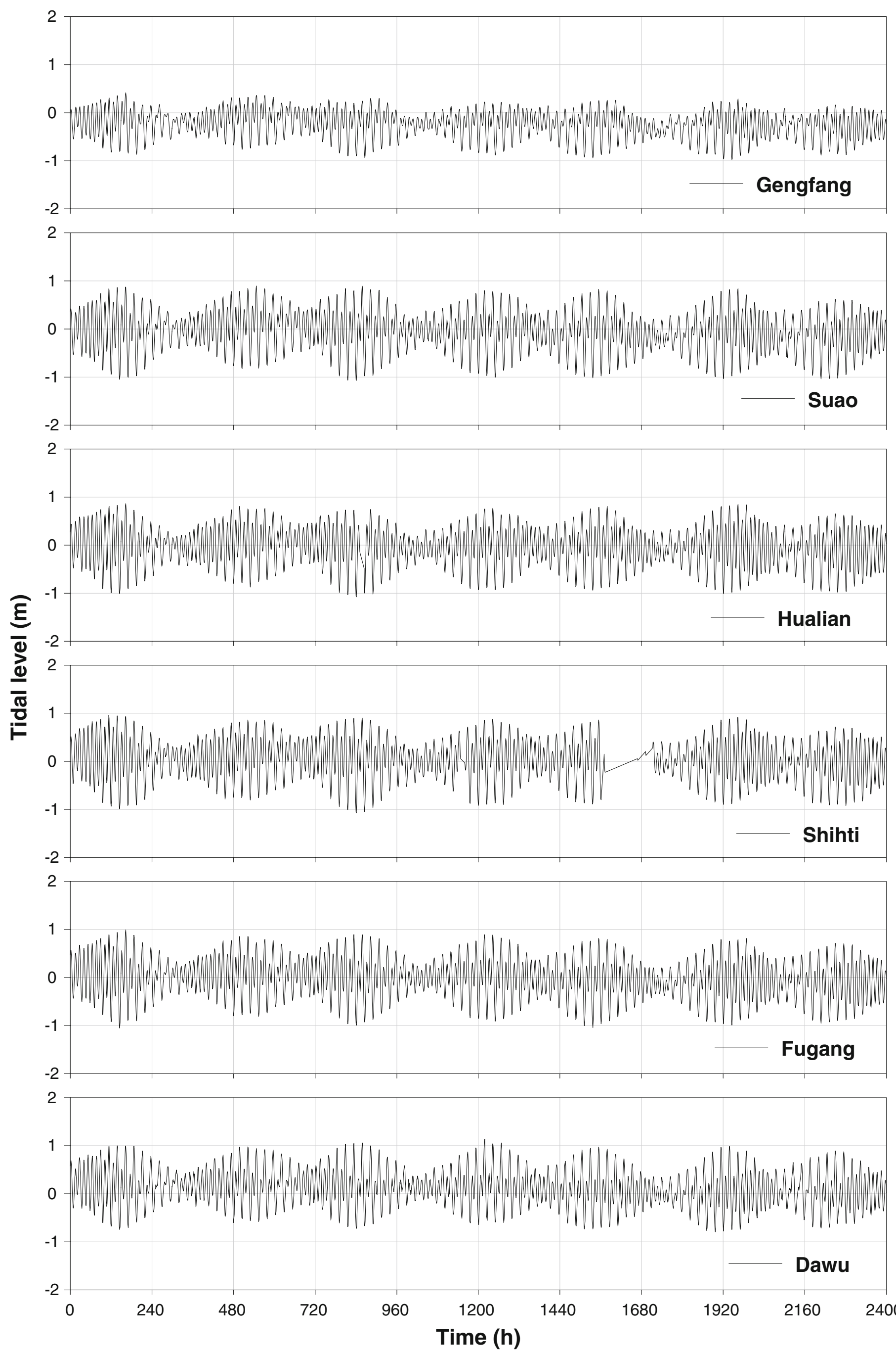

Fig. 2 Hourly time series represented for the winter sea level

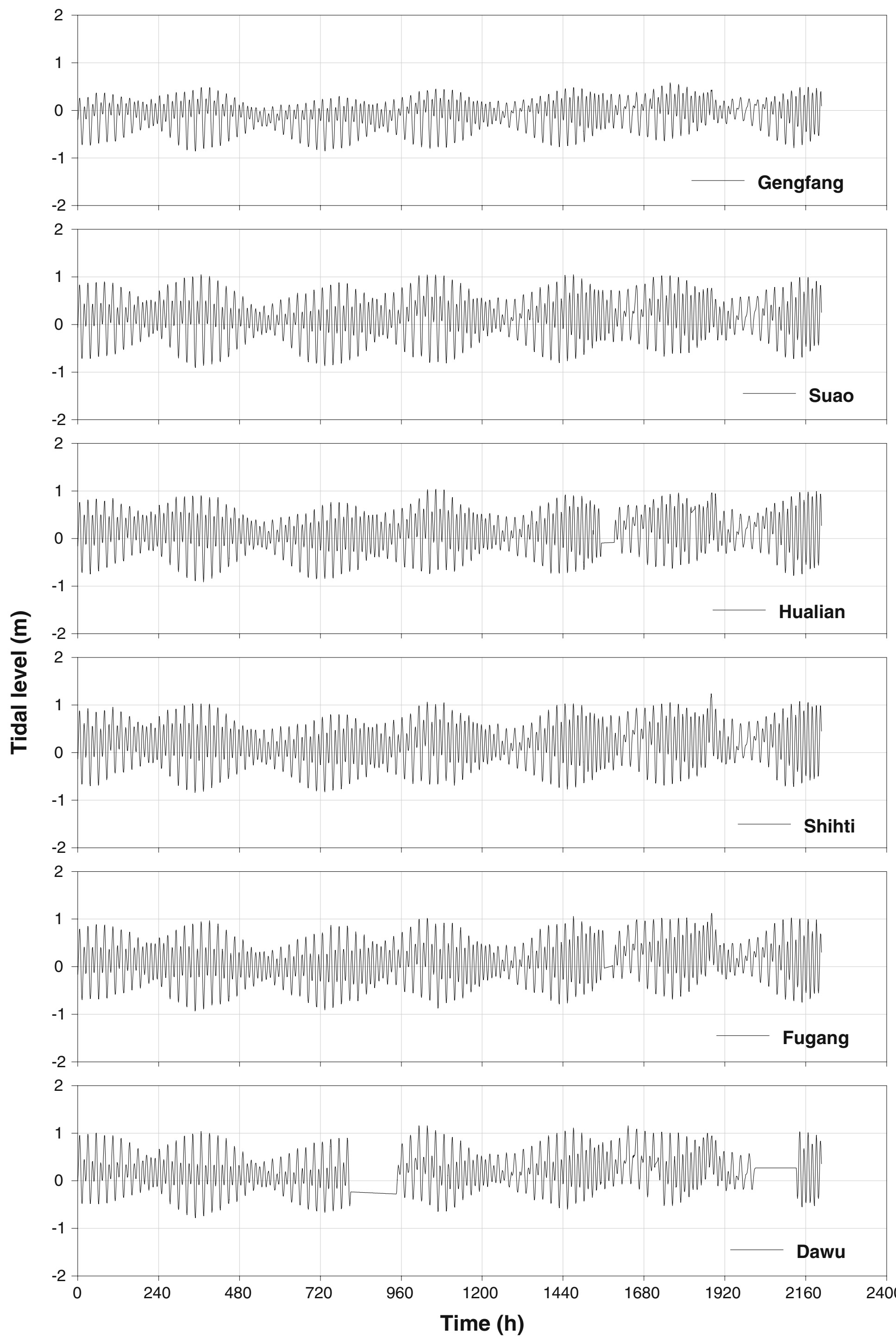

Fig. 3 Hourly time series represented for the summer sea level

potential candidate area which can be used for pilot study or in-situ testing. It can be expected that east coast of Taiwan will be the operated area for transport of CO_2 from main islands to that target area. This study is a preliminary research to identify tidal sea level fluctuations over the east coast of Taiwan. Descriptive statistical assessment is used to describe quantitative data. Variations are analyzed by selecting time series in the cases of winter and summer. Systematic displays of periodic components in tidal gauge have been analyzed using spectral analysis with pre-defined statistical significance. Results of assessment can be provided as a basis for planning work of ocean engineering in the future.

Table 2 Descriptive statistics and normality test for winter sea level, 2006

Station	Size	Mean	Std. dev.	Std. error	C.I. of mean
Gengfang	2,880	−0.2330	0.268	0.00500	0.0098
Suao	2,880	−0.0459	0.402	0.00749	0.0147
Hualian	2,880	−0.0354	0.395	0.00737	0.0144
Shihti	2,880	0.0275	0.400	0.00745	0.0146
Fugang	2,880	−0.0136	0.401	0.00747	0.0146
Dawu	2,880	0.1210	0.372	0.00694	0.0136
	Range	Maximum	Minimum	Median	25%	75%
Gengfang	1.391	0.418	−0.973	−0.205	−0.411	−0.039
Suao	1.993	0.920	−1.073	−0.027	−0.315	0.238
Hualian	1.999	0.919	−1.080	−0.017	−0.305	0.261
Shihti	2.032	0.957	−1.075	0.035	−0.228	0.321
Fugang	2.046	0.991	−1.055	−0.006	−0.279	0.272
Dawu	1.928	1.132	−0.796	0.113	−0.133	0.370
	Skewness	Kurtosis	K-S dist.	K-S prob.	Sum	Sum of squares
Gengfang	−0.385	−0.349	0.0515	<0.001	−670.176	363.447
Suao	−0.188	−0.379	0.0231	0.001	−132.066	470.942
Hualian	−0.208	−0.497	0.0304	<0.001	−101.891	453.886
Shihti	−0.187	−0.395	0.0215	0.004	79.193	461.898
Fugang	−0.105	−0.444	0.0167	0.061	−39.117	462.944
Dawu	0.078	−0.356	0.0147	0.152	347.670	441.103
	Normality test					
Gengfang	K-S Dist. = 0.051	$P < 0.001$	Failed			
Suao	K-S Dist. = 0.023	$P = 0.001$	Failed			
Hualian	K-S Dist. = 0.030	$P < 0.001$	Failed			
Shihti	K-S Dist. = 0.021	$P = 0.004$	Failed			
Fugang	K-S Dist. = 0.017	$P = 0.061$	Passed			
Dawu	K-S Dist. = 0.015	$P = 0.152$	Passed			

Table 3 Descriptive statistics and normality test for summer sea level, 2007

Station	Size	Mean	Std. dev.	Std. error	C.I. of mean
Gengfang	2,208	−0.076	0.2.82	0.00599	0.0117
Suao	2,208	0.152	0.402	0.00855	0.0168
Hualian	2,208	0.131	0.390	0.00830	0.0163
Shihti	2,208	0.181	0.412	0.00877	0.0172
Fugang	2,208	0.115	0.4.07	0.00866	0.0170
Dawu	2,208	0.185	0.373	0.00795	0.0156
	Range	Maximum	Minimum	Median	25%	75%
Gengfang	1.437	0.582	−0.855	−0.0380	−0.245	0.128
Suao	1.955	1.049	−0.906	0.1710	−0.110	0.438
Hualian	1.954	1.039	−0.915	0.1385	−0.131	0.428
Shihti	2.081	1.240	−0.841	0.1970	−0.107	0.497
Fugang	2.058	1.123	−0.935	0.1175	−0.171	0.402
Dawu	1.939	1.159	−0.780	0.1910	−0.083	0.413
	Skewness	Kurtosis	K-S dist.	K-S prob.	Sum	Sum of squares
Gengfang	−0.469	−0.263	0.0563	<0.001	−168.654	187.726
Suao	−0.194	−0.413	0.0225	0.011	335.759	407.125
Hualian	−0.183	−0.514	0.0341	<0.001	289.446	373.703
Shihti	−0.125	−0.602	0.0336	<0.001	400.386	447.272
Fugang	−0.040	−0.488	0.0189	0.064	253.573	394.233
Dawu	0.162	−0.403	0.0338	<0.001	407.865	383.013
	Normality test					
Gengfang	K-S dist. = 0.056	$P < 0.001$	Failed			
Suao	K-S dist. = 0.023	$P = 0.011$	Failed			
Hualian	K-S dist. = 0.034	$P < 0.001$	Failed			
Shihti	K-S dist. = 0.034	$P < 0.001$	Failed			
Fugang	K-S dist. = 0.019	$P = 0.064$	Passed			
Dawu	K-S dist. = 0.034	$P < 0.001$	Failed			

2 Conceptual model of research

There are six tide gauge stations (Table 1) aligned on the east of Taiwan; this boundary is located exactly on the break of continental shelf on the southeast of Eurasian Plate (Fig. 1). Topographically, depth variation is quite complicated from north to south for Okinawa Backarc Basin to Luzon Arc. This research is mainly to analyze significant tidal components of seasonal sea level and to identify phase propagation of such variations along this boundary line. Time series data acquired hourly sea level samples of 2880 in winter and 2208 in summer for the duration from November 2006 to February 2007 and from July to August 2007, respectively. Note that a couple of significant periodic components have demonstrated on the resultant time series representations for winter and summer (Figs. 2, 3). Sea level fluctuations are nearly within a range of ±1.2 m (Tables 2, 3). Mean sea level and median in sample were also higher in the summer than in the winter for all stations. This implies that the average sea level is higher in summer than in winter, subjected to the zero sea level.

3 Spectral analysis

Spectral analysis is a useful method to evaluate characteristics of the time series periodic fluctuation in

Fig. 4 Autospectral density for the winter sea level. Semidiurnal, diurnal, and tri-diurnal components are represented

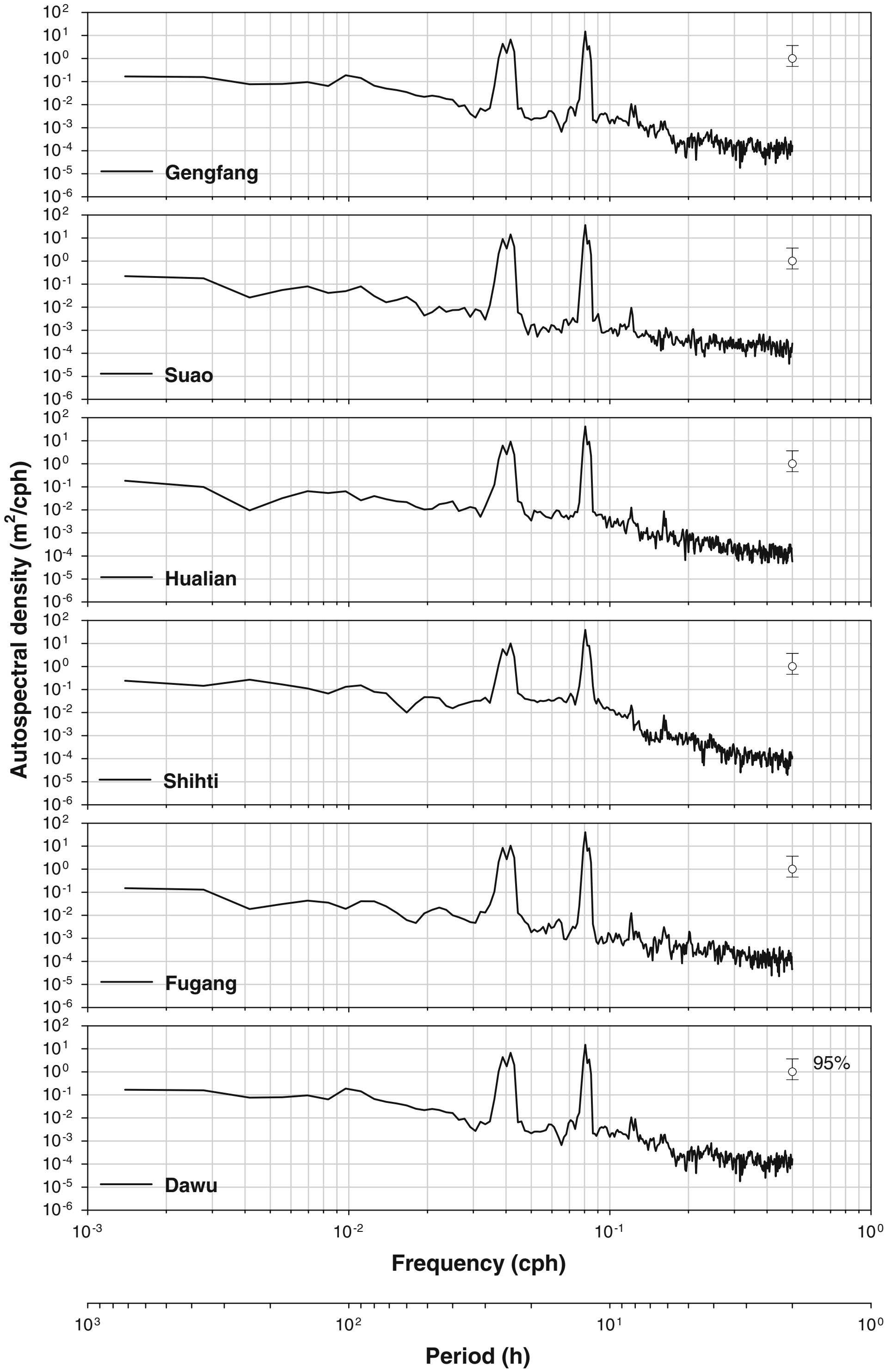

frequency domain. Practical presentation of the spectral techniques can be seen in Bendat and Piersol (2000). Shih has a wide application of spectral analysis to identify fluctuation frequency and phase propagation in tidal water level of aquifers and river (Shih et al. 1999; Shih et al. 2000, 2002; Shih 2002). Autospectral density function is used to detect the stronger signal in time series while cross-spectral density and coherence are measured to identify intensity of specific components between two time series. The 95% confidence interval for autospectral density function and non-zero coherence level for cross-spectral density function can also evaluate significant

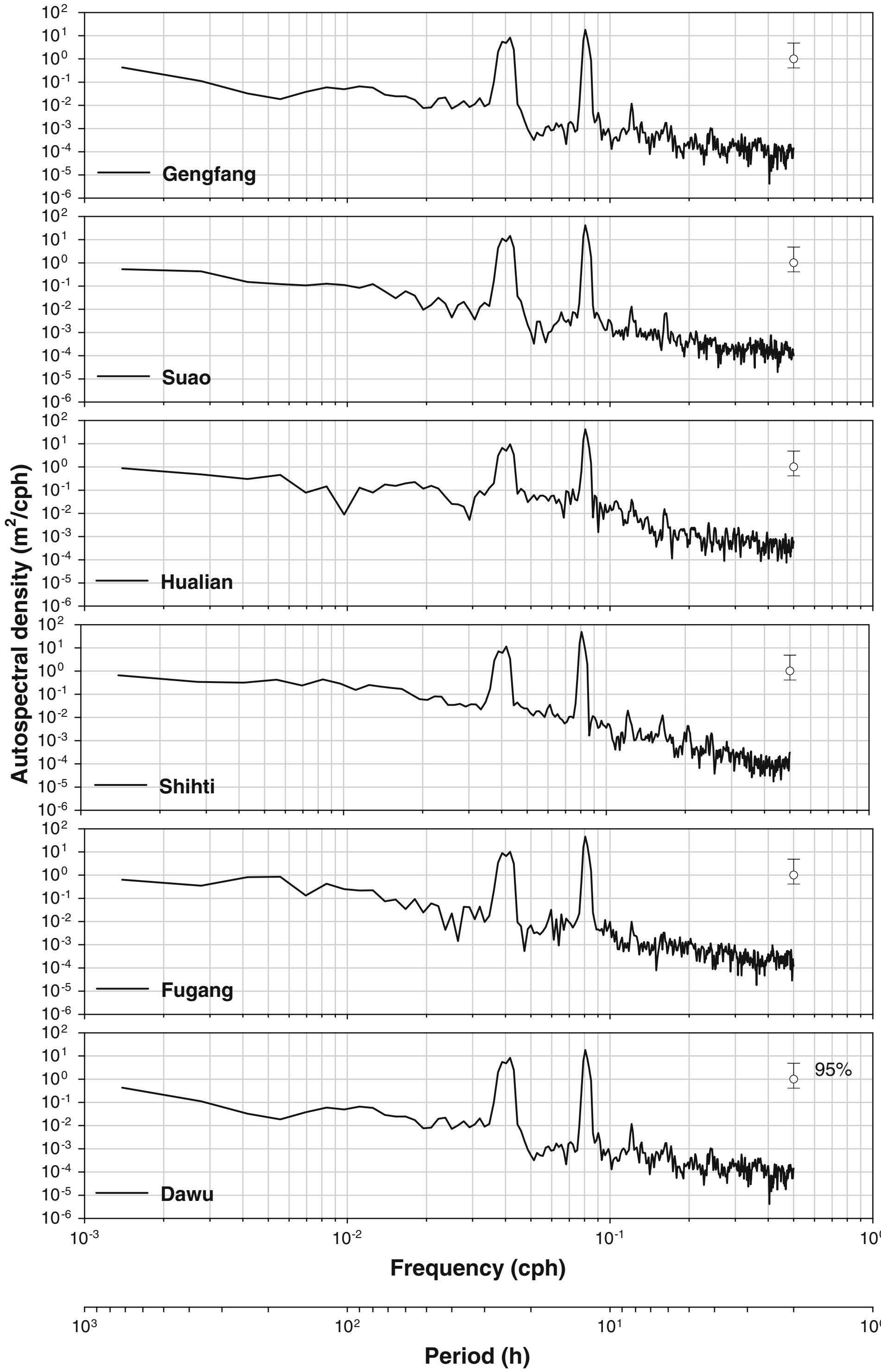

Fig. 5 Autospectral density for the summer sea level. Semidiurnal, diurnal, and tri-diurnal components are represented as significant peaks

components in frequency domain. Basic development of spectral analysis and its extended application in tidal hydrological aspects can be demonstrated in relevant references (Bendat and Piersol 2000; Shih et al. 1999, 2000; Shih and Lin 2002; Shih 2002). The methodology of stationary spectral analysis can be found in detail in the updated work of Bendat and Piersol (2000). Many advanced applications in geosciences for obtaining spectral estimates are also found in the relevant studies (Shih et al. 1999, 2000; Shih 1999a, b, 2000, 2002; Shih and

Table 4 Spectral analysis for winter sea level, 2006

Period	Autospectral density (m^2/cph)		Spectral density (m^2/cph)			Coherence	Phase angle (degree)	Time lag		Leading type
			Co-	Quadrature	Cross			h	min	
12.414 h										
Gengfang–Suao	1.4900E+01	3.6871E+01	2.2657E+01	−5.9347E+00	2.3422E+01	0.99926	−14.6780	−0.50613	−30.3678	Gengfang lead Suao
Suao–Hualian	3.6871E+01	4.1659E+01	3.9076E+01	2.3600E+00	3.9147E+01	0.99885	3.4563	0.11918	7.1508	Suao lag Hualian
Hualian–Shihti	4.1659E+01	3.9266E+01	3.9646E+01	−5.8641E+00	4.0077E+01	0.99091	−8.4137	−0.29013	−17.4078	Hualian lead Shihti
Shihti–Fugang	3.9266E+01	4.0225E+01	3.9231E+01	4.4219E+00	3.9479E+01	0.99336	6.4310	0.22176	13.3056	Shihti lag Fugang
Fugang–Dawu	4.0225E+01	3.1057E+01	3.5291E+01	−7.5066E−02	3.5291E+01	0.99848	−0.1219	−0.00420	−0.2521	Fugang lead Dawu
24.000 h*										
Gengfang–Suao	6.7105E+00	1.4366E+01	9.7245E+00	1.2165E+00	9.8003E+00	0.99815	7.1307	0.47538	28.5228	Gengfang lag Suao
Suao–Hualian	1.4366E+01	9.2129E+00	1.1416E+01	−1.2966E+00	1.1489E+01	0.99867	−6.4801	−0.43201	−25.9206	Suao lead Hualian
Hualian–Shihti	9.2129E+00	1.0105E+01	9.4868E+00	−3.8753E−01	9.4947E+00	0.98403	−2.3392	−0.15595	−9.3570	Hualian lead Shihti
Shihti–Fugang	1.0105E+01	1.0585E+01	9.9358E+00	2.4406E+00	1.0231E+01	0.98924	13.8010	0.92004	55.2024	Shihti lag Fugang
Fugang–Dawu	1.0585E+01	1.1411E+01	1.0824E+01	1.8110E+00	1.0975E+01	0.99859	9.4984	0.63323	37.9938	Fugang lag Dawu
8.276 h										
Gengfang–Suao	1.0652E−02	9.4146E−03	9.6358E−03	1.9374E−04	9.6378E−03	0.96241	1.1519	0.02648	1.5888	Gengfang lag Suao
Suao–Hualian	9.4146E−03	1.2602E−02	8.3940E−03	2.6963E−03	8.8164E−03	0.80941	17.8080	0.40938	24.5628	Suao lag Hualian
Hualian–Shihti	1.2602E−02	2.0410E−02	1.4143E−02	−4.7954E−03	1.4934E−02	0.93114	−18.7300	−0.43058	−25.8348	Hualian lead Shihti
Shihti–Fugang	2.0410E−02	1.2400E−02	1.1517E−02	−2.8646E−03	1.1868E−02	0.74600	−13.9680	−0.32109	−19.2654	Shihti lead Fugang
Fugang–Dawu	1.2400E−02	1.4538E−02	1.0479E−02	4.6471E−03	1.1464E−02	0.85378	23.9150	0.54977	32.9862	Fugang lag Dawu

− station pairs; * second peak at 25.714 h [0.038889 cph])

Table 5 Spectral analysis for summer sea level, 2007

Period	Autospectral density (m^2/cph)		Spectral density (m^2/cph)			Coherence	Phase angle (degree)	Time lag		Leading type
			Co-	Quadrature	Cross			h	min	
12.414 h										
Gengfang–Suao	1.8183E+01	4.1621E+01	2.5989E+01	−8.9924E+00	2.7500E+01	0.99967	−19.0860	−0.65815	−39.4890	Gengfang lead Suao
Suao–Hualian	4.1621E+01	4.2509E+01	4.1796E+01	4.4051E+00	4.2028E+01	0.99918	6.0164	0.20746	12.4476	Suao lag Hualian
Hualian–Shihti	4.2509E+01	4.9307E+01	4.4872E+01	−8.7788E+00	4.5723E+01	0.99870	−11.0700	−0.38171	−22.9026	Hualian lead Shihti
Shihti–Fugang	4.9307E+01	4.6048E+01	4.7171E+01	6.5455E+00	4.7623E+01	0.99944	7.9000	0.27241	16.3446	Shihti lag Fugang
Fugang–Dawu	4.6048E+01	2.9528E+01	3.6720E+01	1.4845E−01	3.6720E+01	0.99584	0.2316	0.00799	0.4792	Fugang lag Dawu
24.000 h*										
Gengfang–Suao	8.3668E+00	1.4557E+01	1.1007E+01	7.1970E−01	1.1031E+01	0.99952	3.7410	0.24940	14.9640	Gengfang lag Suao
Suao–Hualian	1.4557E+01	9.6187E+00	1.1693E+01	−1.4860E+00	1.1787E+01	0.99613	−7.2427	−0.48285	−28.9710	Suao lead Hualian
Hualian–Shihti	9.6187E+00	1.1571E+01	1.0519E+01	−1.7939E−01	1.0521E+01	0.99726	−0.9770	−0.06513	−3.9079	Hualian lead Shihti
Shihti–Fugang	1.1571E+01	1.0198E+01	1.0381E+01	3.1339E+00	1.0844E+01	0.99820	16.7980	1.11990	67.1940	Shihti lag Fugang
Fugang–Dawu	1.0198E+01	1.0009E+01	1.0014E+01	8.3826E−01	1.0049E+01	0.99466	4.7849	0.31900	19.1400	Fugang lag Dawu
8.276 h										
Gengfang–Suao	1.1732E−02	1.3049E−02	1.0400E−02	2.3420E−03	1.0660E−02	0.86157	12.6910	0.29175	17.5050	Gengfang lag Suao
Suao–Hualian	1.3049E−02	3.9026E−02	1.9803E−02	−6.1447E−03	2.0735E−02	0.91882	−17.2380	−0.39628	−23.7768	Suao lead Hua-lian
Hualian–Shihti	3.9026E−02	1.9620E−02	2.5497E−02	1.1196E−03	2.5521E−02	0.92229	2.5143	0.05780	3.4680	Hualian lag Shihti
Shihti–Fugang	1.9620E−02	9.7880E−03	9.9049E−03	−3.4235E−04	9.9108E−03	0.71517	−1.9796	−0.04551	−2.7304	Shihti lead Fugang
Fugang–Dawu	9.7880E−03	1.4652E−02	2.1115E−03	−8.5511E−03	8.80800−03	0.73550	−76.1290	−1.75010	−105.0060	Fugang lead Dawu

− station pairs; * second peak at 25.714 h [0.038889 cph])

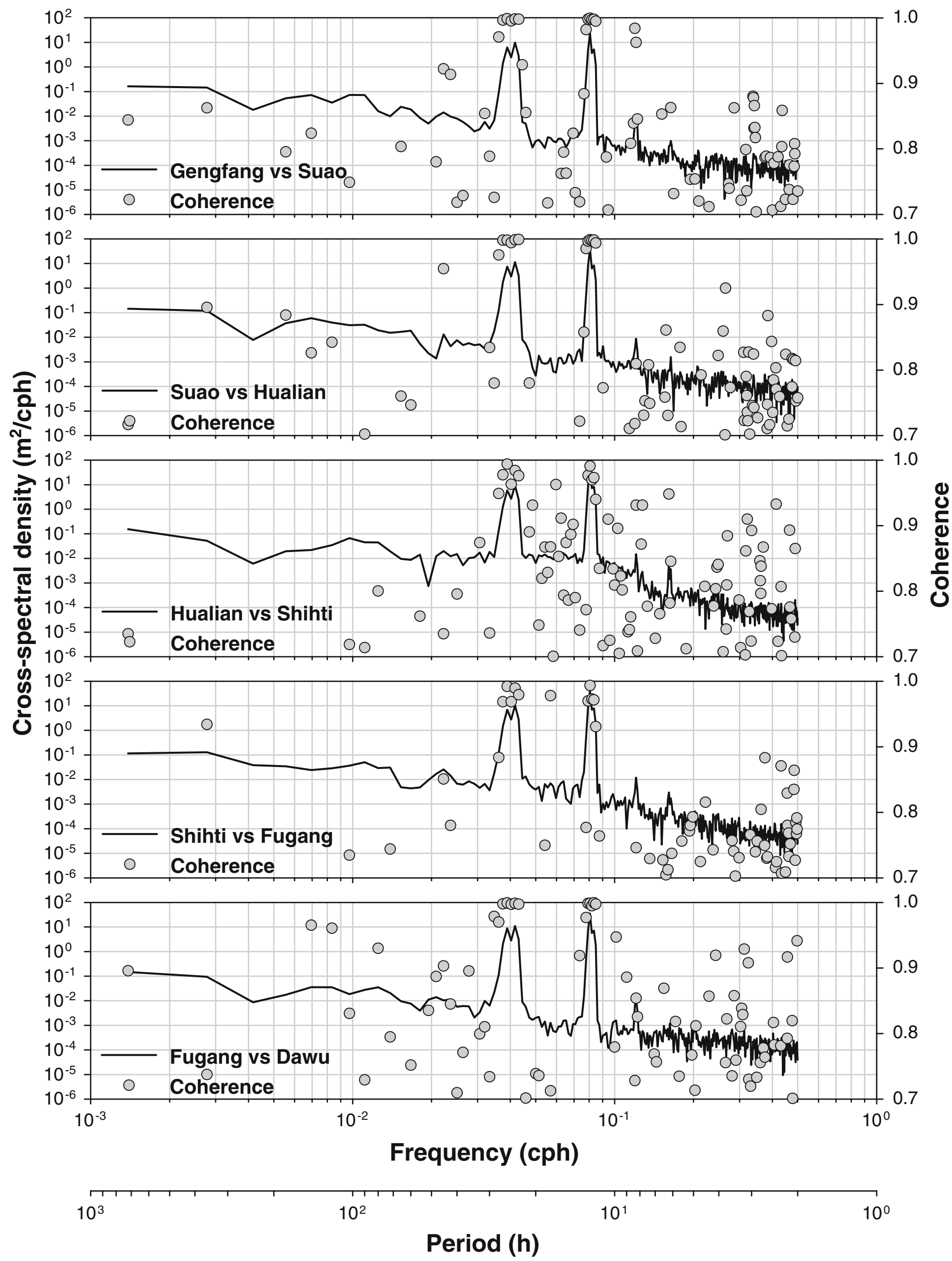

Fig. 6 Cross-spectral density and coherence for station pair in the winter. Significant coherence for semidiurnal, diurnal, and tri-diurnal components are demonstrated in order

Lin 2002, 2004; Shih 2008; Shih et al. 2008a, b). Detailed procedure and computation for spectral analysis can be reviewed on the above-mentioned studies.

4 Result and discussion

It uses Kolmogorov–Smirnov normality test (Eadie et al. 1971; Stuart et al. 1999) to inspect normality status of the studied time series data (Tables 2, 3). If the time series variables fail the normality test, it implies that manipulating non-stationary time series data for stationary spectral analysis is needed. In order to reduce the random error of the spectral density function, the data are separated and independently calculated by a length of 720 h each time to obtain a smooth estimate using continuous segments. It implies that periodic components greater than 30 days is restrained. Such manipulation is enough to present the stationary part and overcome the failure of normality test in that period. To suppress the temporal variation in the time series data, removal of the linear trend is adopted on each segment using the least-squares method,

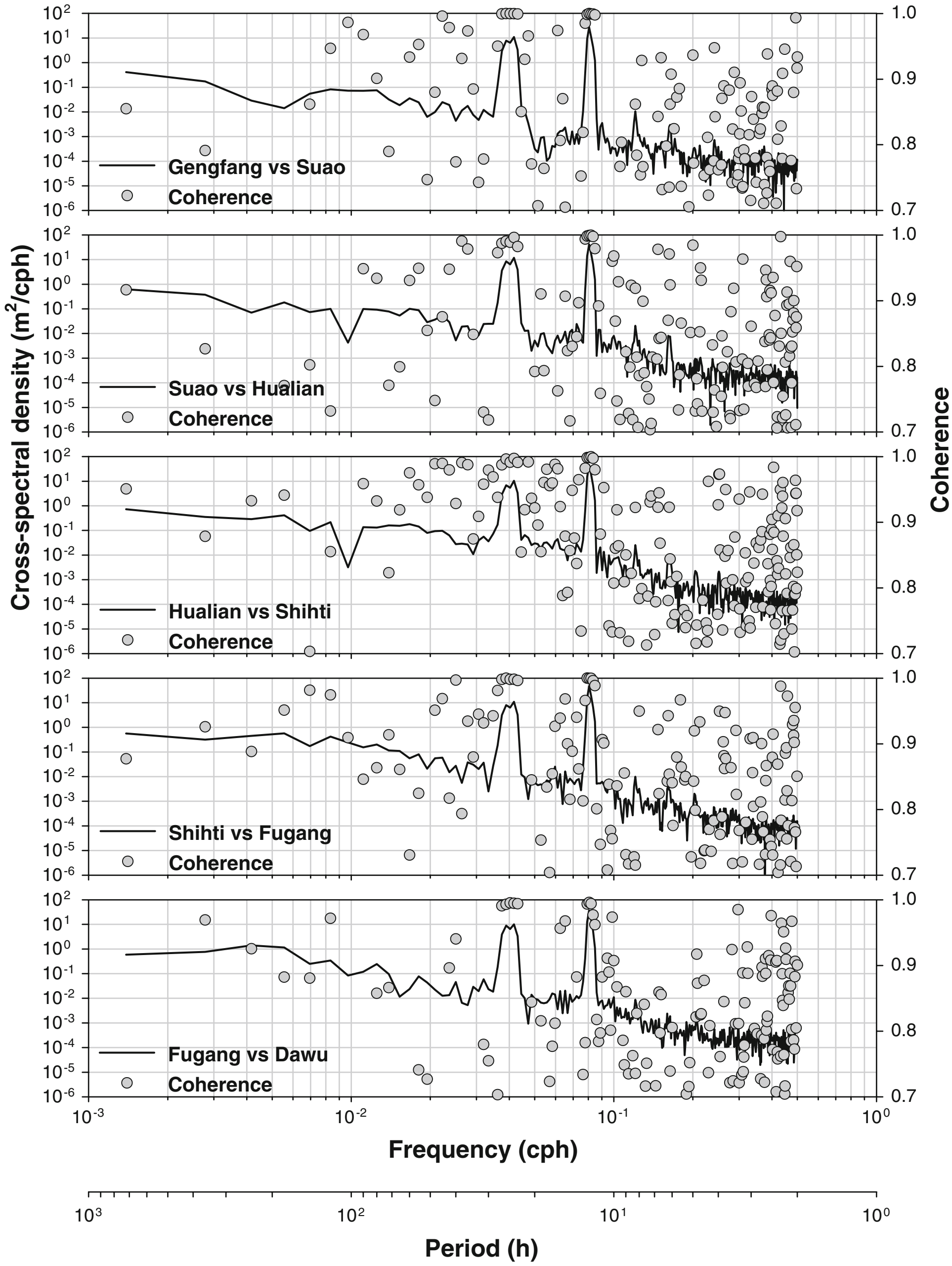

Fig. 7 Cross-spectral density and coherence for station pair in the summer. Significant coherence for semidiurnal, diurnal, and tri-diurnal components are demonstrated in order

while the Hanning window is used to suppress the leakage problem (Bloomfield 1976). The discrete frequency resolution is set to be 0.13889×10^{-2} Hz. The autospectral density with 95% confidence interval has lower and the upper extremes of 0.41524 and 4.8491, respectively. The non-zero coherence significant level is calculated to be 0.73964. Although the confidence interval of the cross-spectral density function is dependent on coherence at each discrete frequency interval, it is reasonable to evaluate the significant peak in the cross-spectral density function using the non-zero coherence level (NZC) instead of the confidence interval (Shih et al. 1999). For the data from winter and summer, autospectral density shows that the most significant periodic peak is at the period of 12.414 h (0.080556 cph) and the second peak is at 24 h (0.041667 cph) accompanied with 25.714 h (0.038889 cph) (Figs. 4, 5; Tables 4, 5). The third significant peak is demonstrated at the period of 8.276 h (0.12083 cph) which is relatively small comparing with semi-diurnal and diurnal components. In short, they are subjected to the semi-diurnal M_2, diurnal group of K_1 and O_1, and tri-diurnal component of astronomical tide. M_2 tide is the principal

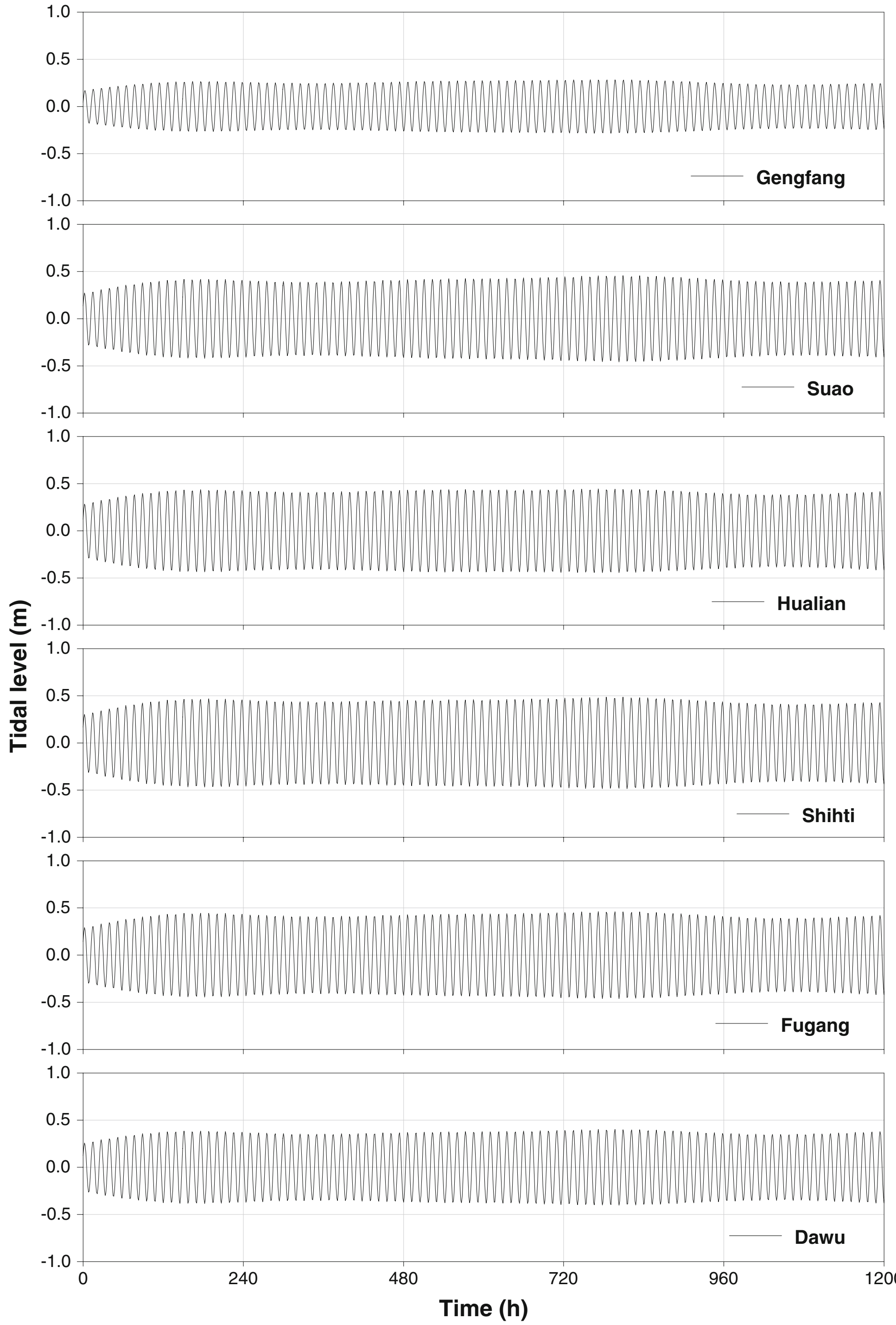

Fig. 8 Hourly time series in the winter using bandpass frequency 0.079167–0.081944 cph for semi-diurnal component

lunar semidiurnal constituent at speed 28.984 degrees per mean solar hour while K_1 and O_1 are luni-solar declinational diurnal constituent at speeds of 15.041 and 13.943 degrees per mean solar hour, respectively (Godin 1972). Six tide gauge stations forming five station pairs are selected for analysis of the coherence and phase propagation from north to south including evaluation of cross spectral density in frequency domain (Figs. 6, 7; Tables 4, 5). It represents drastically high coherence for semi-diurnal and diurnal components in the station pairs from north to south in winter and summer (Tables 4, 5). Note that the semidiurnal components from Fugang and Dawu stations are nearly in phase both in winter and summer, and the leading types are similar through the year for all station

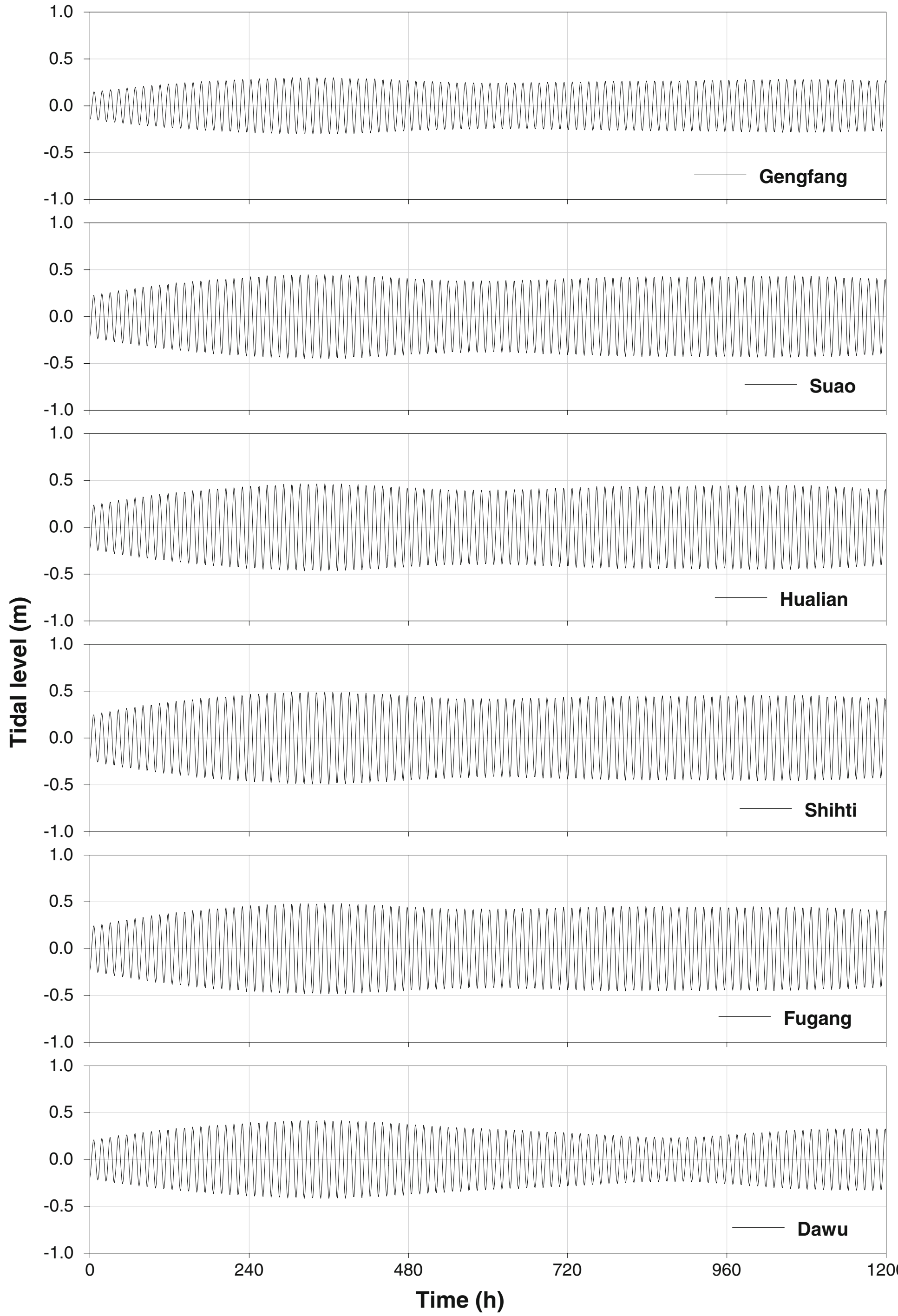

Fig. 9 Hourly time series in the summer using bandpass frequency 0.079167–0.081944 cph for semi-diurnal component

pairs. Cross-spectral density of diurnal components for Gengfang-Suao pair in the summer demonstrate double time lag as compared to that in the winter; the leading types are also similar through the year for all station pairs. Figures 8–13 shows that resultant time series have manipulated using relevant filter for semi-diurnal, diurnal, and tri-diurnal components, respectively. All of them are limited in a one-meter range, i.e. a half meter about zero mean. It shows that semi-diurnal component has enveloped in the winter and summer for Dawu station (Figs. 8, 9). Especially, it demonstrates that diurnal component has enveloped with the period of 14 days in the winter and summer (Figs. 10, 11). Quite different variations for tri-diurnal component have also been found using a bandpass

Fig. 10 Hourly time series in the winter using bandpass frequency at 0.037500–0.043056 cph for diurnal component

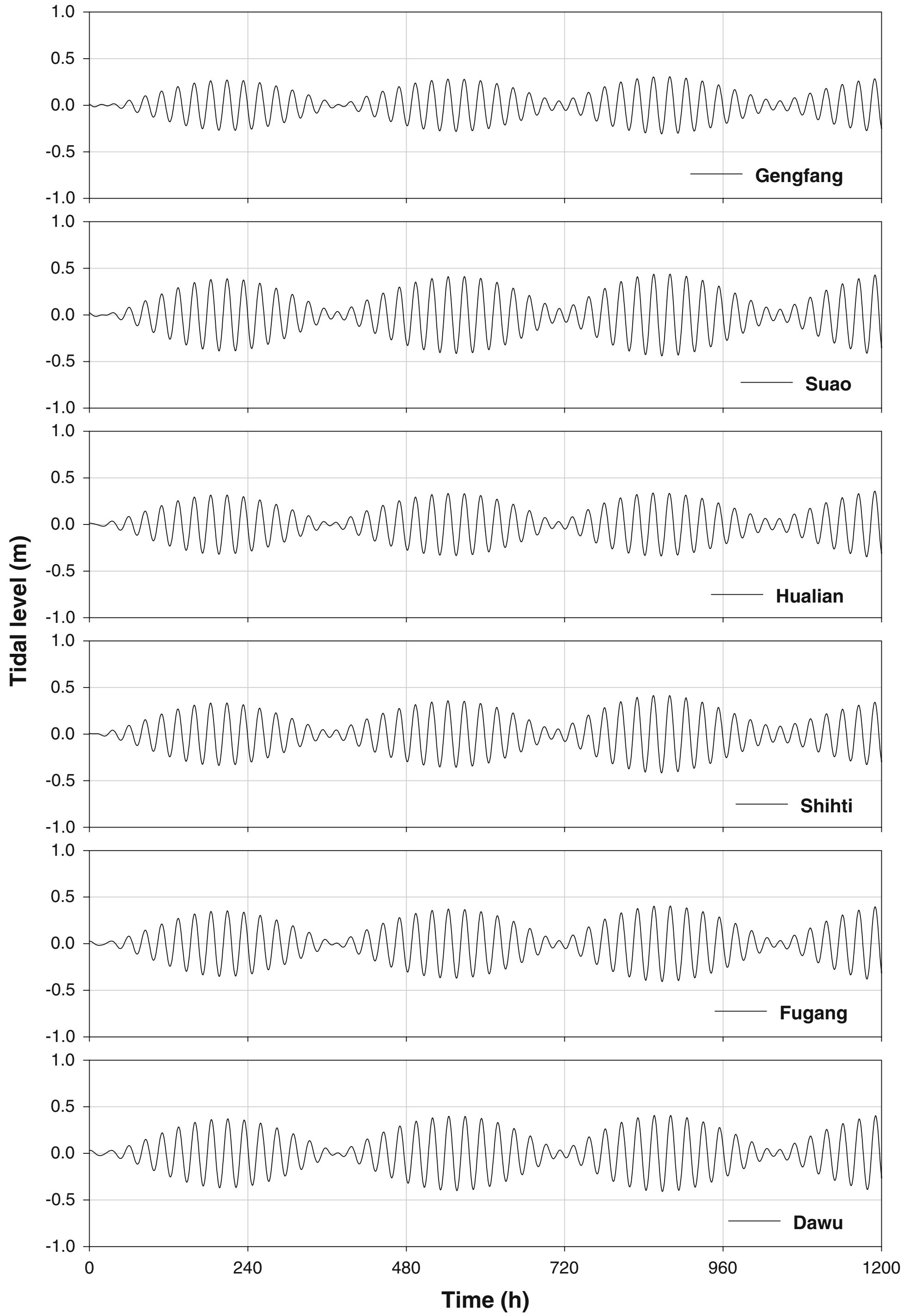

frequency of 0.11944–0.12222 cph (Figs. 12, 13). The less energy in cross-spectral density indicate different fluctuation in some degree for the lower frequency related to 3–8 days, or a period of 70–200 h (Figs. 6, 7). In the winter, time lag for all station pairs are nearly bounded in 30 min for semi-diurnal component while 1 h for diurnal component; tri-diurnal component is nearly restricted in a half hour (Table 4). In the summer, time lag for all station pair is nearly bounded in 40 min for semi-diurnal component while 70 min for diurnal component; tri-diurnal component is nearly restricted in 105 min (Table 5). It also represents that Fugang and Dawu for semidiurnal and Shiti and Hualian for diurnal component are almost in phase both in winter and summer (Tables 4 and 5). It shows that two

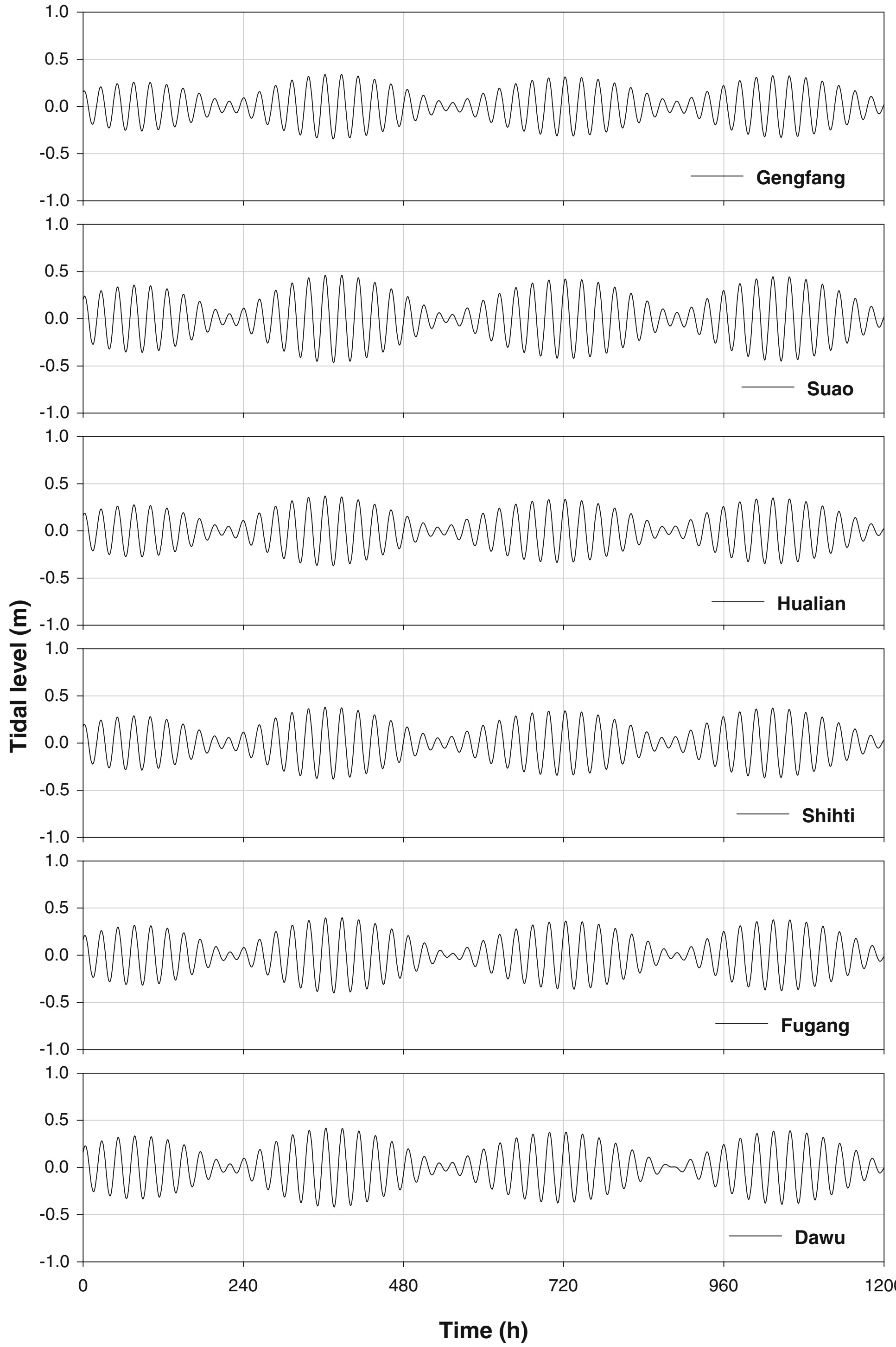

Fig. 11 Hourly time series in the summer using bandpass frequency at 0.037500–0.043056 cph for diurnal component

significant constituents related to astronomical tidal fluctuations have been found, i.e. semi-diurnal and diurnal components.

Transport and meandering period has been investigated using sub-inertial and temperature variance (Zhang et al. 2001). Approximately 60% of the total sub-inertial velocity and temperature variance in the Kuroshio east of Taiwan is associated with so-called "transport" and "meandering" modes revealed from empirical orthogonal function analysis. The transport mode is dominated by a 100-day peak, while the most coherent energetic meandering signals are found in three limited frequency bands centered near

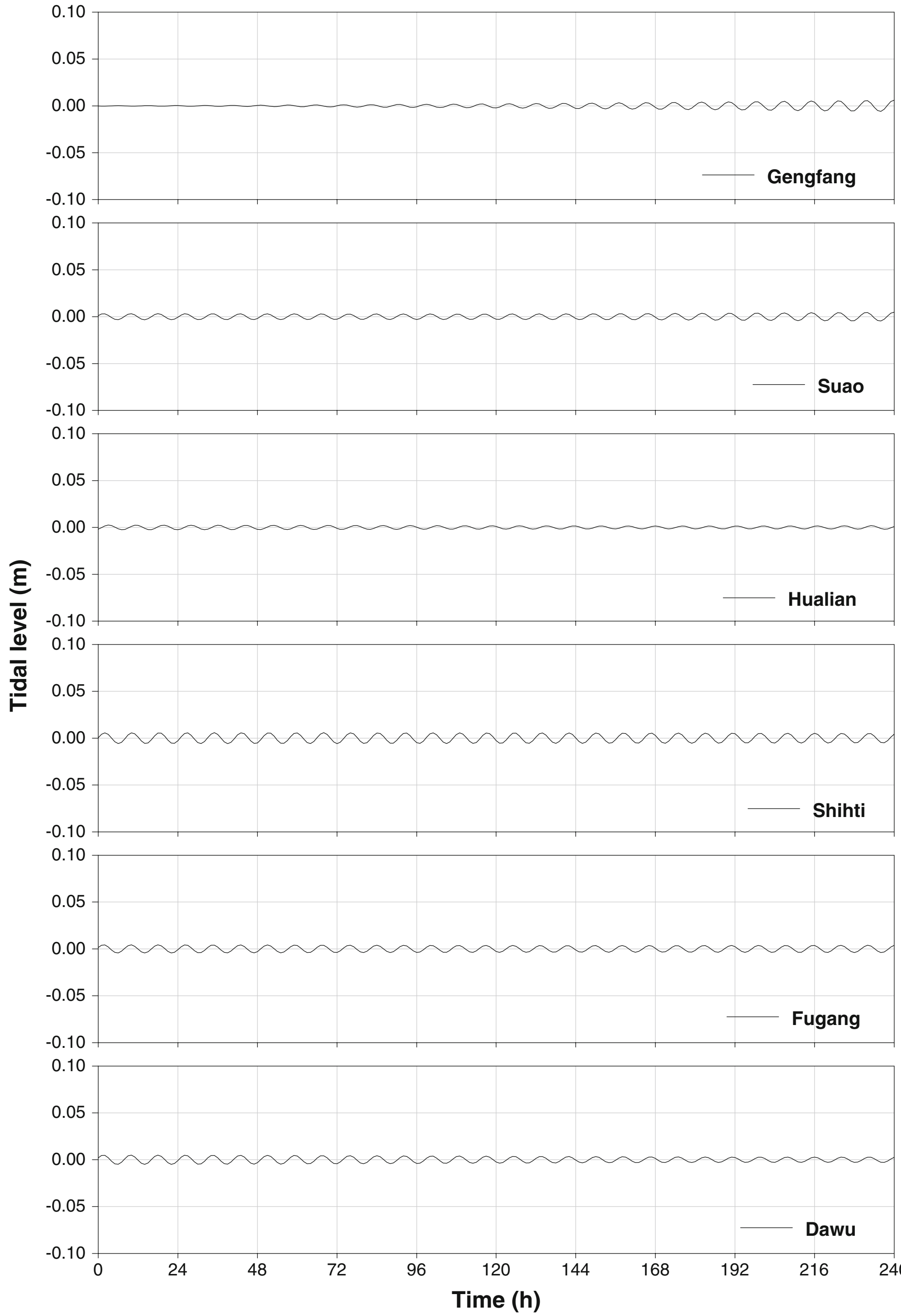

Fig. 12 Hourly time series in the winter using bandpass frequency at 0.119440–0.122220 cph for tri-diurnal component

periods of 100, 40, and 18 days. These signals are obviously different from the tidal sea level studied for the east coast of Taiwan associated to the period less than the diurnal time scale.

Commonly, there are four methods considered for CO_2 injection: (1) a vertical pipe attached to an oil platform; (2) a submerged tank; (3) a flexible pipe tethered to a moving ship; and (4) a pipe installed along the ocean floor. The CO_2 delivery concept was drastically changed, moving from a shore-based CO_2 storage facility (tank) to a floating ship. By moving offshore, impacts on any rugged and environmentally sensitive shallower waters would be completely avoided. The condition of tidal sea level is needed to assess suitability

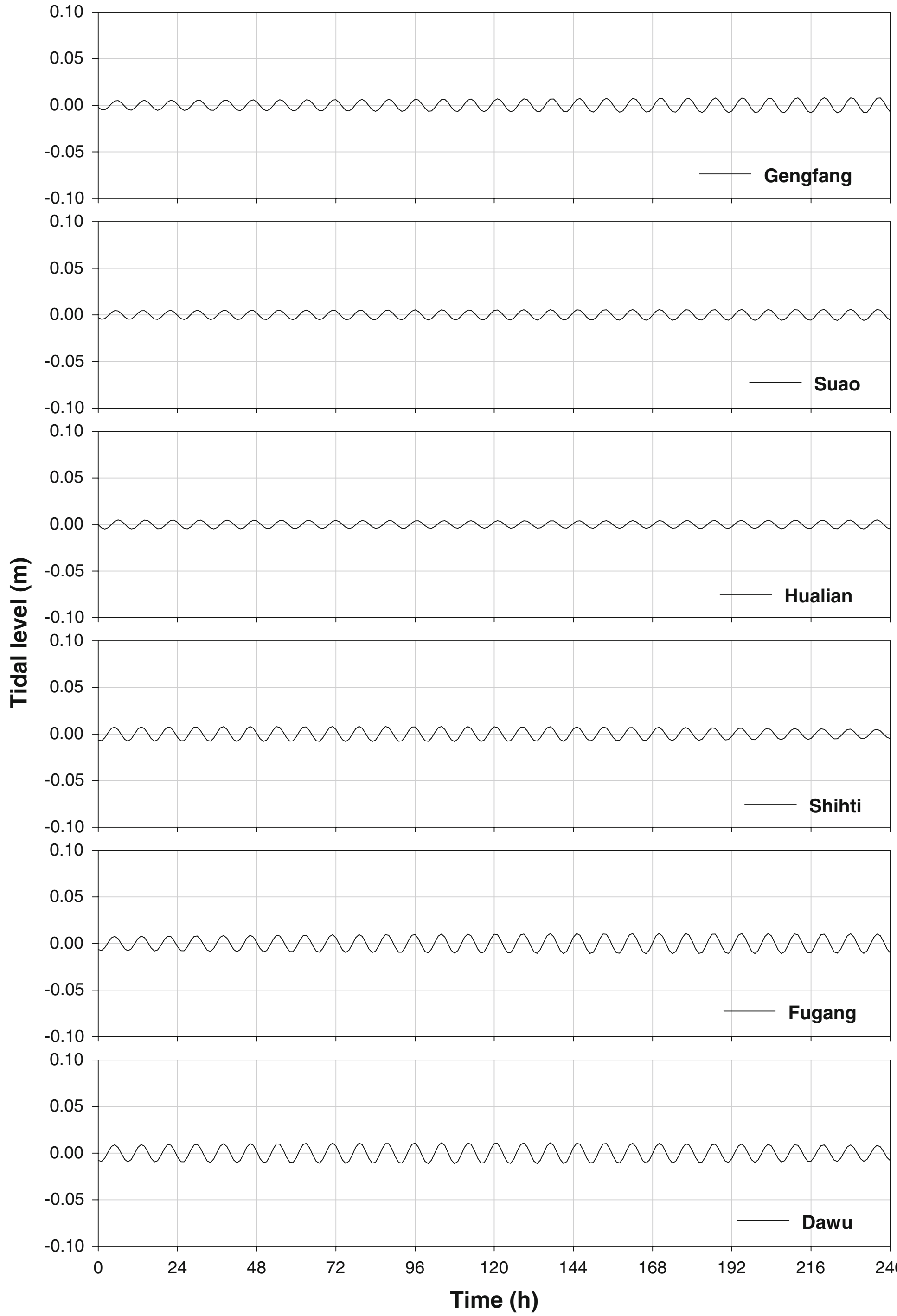

Fig. 13 Hourly time series in the summer using bandpass frequency at 0.119440–0.122220 cph for tri-diurnal component

considering the east coast of Taiwan as a candidate location for temporary storage of CO_2. It describes a completed demonstration of tidal fluctuation on east coast of Taiwan in time and frequency domains; phase and propagation type are also represented. This research provides a fundamental knowledge of tidal fluctuation on shoreline substantially. In the future, more detail phase contour of tidal level offshore around the potential area (122–122.5°E and 21.8–22.3°N) would need to be established accordingly.

5 Conclusions

In order to mitigate carbon dioxide to prevent serious environmental impact of warm house effect, direct CO_2 injection to ocean is one of several options under consideration. For the preliminary judgment, marine regions between 122–122.5°E and 21.8–22.3°N appear to be potential areas, regardless of medium depth or deep sea sequestration. The east of Taiwan can be expected to be the suggested location for CO_2 temporary storage or transported plant. Stability of ocean engineering facility on sea surface will be the critical problem while constructing preliminary testing site. To have whole assessment of sea level fluctuation, seasonal sea level of six tidal gauge stations are collected and analyzed using spectral analysis in time-frequency domain. It gives a statistical summary of seasonal sea level data in the integrity. Periodic component and phase propagation are also analyzed in time—frequency domain. It found that semi-diurnal and diurnal components are related to astronomical tides M_2, and K_1 and O_1; phase propagation of sea level are also represented as local phenomena, i.e., longer time and larger spatial scale transport such as Kuroshio does not affect these tidal fluctuation at coast for the periods from a few hours to diurnal scale. The research provides a completed demonstration of seasonal sea level on the east coast of Taiwan; resultant significance can be considered as a base for constructing testing or operating facility on sea surface in the future.

Acknowledgments The authors thank Central Weather Bureau of Taiwan for providing useful data. The support from the Department of Geosciences of National Taiwan University and the Institute of Nuclear Energy Research (INER), AEC, of Taiwan are also greatly appreciated. In addition, we also thank Mr. Chang, Ching-Chang Chang and Ms. Fu, Tseng-Chih of INER for their effort in preparing sea level data.

References

Aya I, Kojima R, Yamane K, Brewer PG, Pelter ET (2003) In situ experiments of cold CO_2 release in mid-depth. Proceedings of the international conference on greenhouse gas control technologies, 30th September–4th October, Kyoto, Japan

Bendat JS, Piersol AG (2000) Random data, analysis and measurement procedures. Wiley, New York

Bloomfield P (1976) Fourier analysis of time series: an introduction. Wiley, New York

Brewer PG, Orr FM Jr, Friederich G, Kvenvolden KA, Orange DL (1998) Gas hydrate formation in the deep-sea: in situ experiments with controlled release of methane, natural gas and carbon dioxide. Energy Fuels 12(1):183–188

Brewer PG, Peltzer ET, Friederich G, Aya I, Yamane K (2000) Experiments on the ocean sequestration of fossil fuel CO_2: pH measurements and hydrate formation. Mar Chem 72(2–4):83–93

Brewer PG, Peltzer ET, Friederich G, Rehder G (2002) Experimental determination of the fate of a CO_2 plume in seawater. Environ Sci Technol 36(24):5441–5446

Brewer PG, Peltzer ET, Walz P, Aya I, Yamane K, Kojima R, Nakajima Y, Nakayama N, Haugan P, Johannessen T (2005) Deep Ocean experiments with fossil fuel carbon dioxide: creation and sensing of a controlled plume at 4 km depth. J Mar Res 63(1):9–33

Eadie WT, Drijard D, James FE, Roos M, Sadoulet B (1971) Statistical methods in experimental physics. North-Holland, Amsterdam 269–271

Godin G (1972) The analysis of tides. University of Toronto Press, Toronto

IPCC (2005) IPCC special report on carbon dioxide capture and storage. In: Metz B, Davidson O, de Coninck H, Loos M, Meyer L (ed) Published for the Intergovernmental Panel on Climate Change. Cambridge University Press, New York

Nakashiki N (1997) Lake-type storage concepts for CO_2 disposal option. Proceedings from the international symposium on ocean disposal of carbon dioxide. Waste management. An international journal of industrial, hazardous and radioactive waste management, science and technology. October/November 1996, Tokyo, Japan

Ozaki M (1997) CO_2 injection and dispersion in mid-ocean depth by moving ship. Proceedings from the international symposium on ocean disposal of carbon dioxide. Waste management. An international journal of industrial, hazardous and radioactive waste management, science and technology. October/November 1996, Tokyo, Japan

Shih DCF (1999a) Determination of hydraulic diffusivity of aquifers by spectral analysis. Stoch Environ Res Risk A 13(1/2):85–99

Shih DCF (1999b) Inverse solution of hydraulic diffusivity determined by water level fluctuation. J Am Water Resour Assoc 35(1):37–47

Shih DCF (2000) Applicability of spectral analysis to determine hydraulic diffusivity. Stoch Environ Res Risk A 14(2):91–108

Shih DCF (2002) Identification of phase propagation of water level in Tidal River by spectral analysis. Stoch Environ Res Risk A 16(6):449–463

Shih DCF (2008) Wind characterization and potential assessment using spectral analysis. Stoch Environ Res Risk Assess 22(2):247–256

Shih DCF, Lin GF (2002) Spectral analysis of water level in aquifers. Stoch Environ Res Risk A 16(5):374–398

Shih DCF, Lin GF (2004) Application of spectral analysis to determine hydraulic diffusivity of a sandy aquifer (Pingtung County, Taiwan). Hydrol Process 18:1655–1669

Shih DCF, Chiou KF, Lee CD, Wang IS (1999) Spectral responses of water level in tidal river and groundwater. Hydrol Process 13:889–911

Shih DCF, Lee CD, Chiou KF, Tsai SM (2000) Spectral analysis of tidal fluctuations in ground water level. J Am Water Resour Assoc 36(5):1087–1099

Shih DCF, Wu YM, Lin GF, Hu JC, Chen YG, Chang CH (2008a) Assessment of long-term variation in displacement for a GPS site adjacent to a transition zone between collision and subduction. Stoch Environ Res Risk A 22(3):401–410

Shih DCF, Lin GF, Jia YP, Chen YG, Wu YM (2008b) Spectral decomposition of periodic groundwater fluctuation in a coastal aquifer. Hydrol Process 22:1755–1765

Stuart A, Ord K, Arnold S (1999) Kendall's advanced theory of statistics. Arnold, a member of the Hodder Headline Group, London 25.37–25.43

Zhang D, Lee TN, Johns WE (2001) The Kuroshio East of Taiwan: modes of variability and relationship to Interior Ocean Mesoscale Eddies. J Phys Oceanogr 31(4):1031–1053